ENDOR study of Cr^{3+} centers substituting for lithium in lithium niobate

G. Malovichko,[1,*] V. Grachev,[1,†] A. Hofstaetter,[2] E. Kokanyan,[3] A. Scharmann,[2], and O. Schirmer[1]
[1]*Department of Physics, University of Osnabrück, D-49069 Osnabrück, Germany*
[2]*1st Institute of Physics, University of Giessen, D-35392 Giessen, Germany*
[3]*Institute for Physical Researches, Asbtarak, Armenia*

(Received 21 September 2001; revised manuscript received 21 February 2002; published 13 June 2002)

The surroundings of several Cr^{3+} centers in lithium niobate crystals were investigated with the help of electron nuclear double resonance (ENDOR). In order to find optimal conditions for the ENDOR observation a detailed study of these spectra was carried out for a large set of crystals with different chromium concentrations and [Li]/[Nb] ratios. For the main axial Cr_1^{3+} center a full investigation of the ENDOR angular dependencies was performed and the parameters of hyperfine and quadrupole interactions were determined. It is found that Cr^{3+} substitutes for Li^+, however, the chromium ion is shifted by 0.2 Å from the regular Li site. An analysis of quadrupole splitting of ^{53}Cr shows that the parameter of the axial crystal field is negative: $b_2^0 = -0.387\ cm^{-1}$ at 4.2 K. The determined parameters of the hyperfine interactions are several times larger than calculated classical dipole-dipole interactions. The obtained data allowed us to reconstruct the shape and width of the electron paramagnetic resonance (EPR) line in the perfect crystals. The difference between the calculated and observed EPR linewidth can therefore be used for the estimation of the nonstoichiometric crystal imperfection. Rather high values of isotropic (contact) hyperfine interactions demonstrate a transfer of electron density to neighboring nuclei. An analysis of the ENDOR spectra of satellite centers Cr_2^{3+}-Cr_9^{3+} has shown that Cr^{3+} substitutes for Li^+ in these centers also, however, there are strong distortions of electron density distributions caused by the presence of an intrinsic defect in the chromium surroundings. A model with v_{Nb} as a charge compensator of Cr_{Li} center explains most of details of both EPR and ENDOR spectra in a natural way.

DOI: 10.1103/PhysRevB.65.224116 PACS number(s): 76.30.Fc, 76.30.Kg, 77.84.Dy, 76.70.Dx

I. INTRODUCTION

The determination of the structure of centers created in lithium niobate, $LiNbO_3$ (LN), by trivalent ions, including those of transition metals and rare-earth elements, is one of the most important tasks in defect study of this material. Besides pure scientific interest, the elucidation of the position of these impurities in the lattice, their nearest surroundings, and the way of the charge compensation are vital for tailoring fundamental properties of this material for various applications. The discussion about the location of the Cr^{3+} impurity in the crystal lattice started with the first optical and electron paramagnetic resonance (EPR) studies of Cr^{3+} (Refs. 1–4, see Ref. 5 for the introduction to the problem). In this context, one main difficulty is that the most probable positions for impurity incorporation, Li and Nb sites as well as the structural vacancy, have the same local symmetry C_3. This means that they are not distinguishable by many spectroscopic techniques including EPR.

Attempts to determine the impurity positions by indirect methods often gave contradictory information. In pioneering papers[1–3] it was assumed that chromium occupies the Nb site. Later, however, it was concluded on the basis of EPR data[6] that the main axial chromium center characterized by crystal-field parameter $b_2^0 \approx -0.39\ cm^{-1}$ (Cr_1^{3+} center)[5] has to be attributed to Cr on a Li site.

Many of direct methods for the determination of impurity positions are not applicable to the LN:Cr system: Mössbauer spectroscopy[7] demands the presence of special nuclei; channeling investigations (Rutherford backscattering spectrometry, Ref. 8) are more successful in the case of heavy, many-electron ions. Results obtained by an extended x-ray absorption fine structure analysis were in favor of Li substitution,[9] however, these measurements were made for LN crystals with a high dopant level of about 5 mol %, for which clustering and occupation of both Li and Nb positions become very probable. The best fit of the data of particle induced x-ray emission (PIXE) combined with channeling[10] was obtained assuming 60% of the Cr occupying regular Li sites and 40% occupying regular Nb sites. However, this method is not sensitive to the charge state of the impurity and does not distinguish axial C_3 and low-symmetry C_1 satellite centers.[5]

The measurements of the electron nuclear double resonance (ENDOR) are rather complex. However, the ENDOR data give a very rich set of characteristics of hyperfine interactions (HFI) and quadrupole interactions of impurity electrons with own and surrounding nuclei, which can be converted into information about the impurity position, the distribution of electron density, the presence of charge compensators, and so on.

In the ENDOR study[11] of the axial Cr_1^{3+} center in LN crystals, grown from congruent and stoichiometric melts, parameters of hyperfine (49.3 MHz) and quadrupole (−0.37 MHz) interactions for ^{53}Cr were determined. The rather large value of the observed quadrupole interaction was in agreement with the Cr_{Li}^{3+} assignment.

Another chromium center with $b_2^0 \approx 0$ appears in LN codoped with about 6 mol % of Mg. The ENDOR investigations of this center[12,13] showed that the observed hyperfine interactions with several shells of surrounding Li nuclei can be explained by assuming that chromium occupies the Nb site. This was supported by the small value of b_2^0 ($\leqslant 0.01\ cm^{-1}$) and quadrupole interaction (0.1 MHz), more likely to occur for the Nb than for the Li site, and by comparison with

the corresponding parameters[6,11] of the chromium center in LN not codoped with Mg. However, in making a comparison of both types of Cr centers one has to consider: (a) LN without Mg and LN heavily doped with Mg are very different crystals with respect to both the intrinsic and extrinsic defect subsystems; (b) a disappearance of chromium centers with $|b_2^0| \approx 0.39\ \mathrm{cm}^{-1}$ in LN:Mg could be explained, for instance, by the presence of Mg^{2+} in the nearest neighborhood or by the change of charge compensator instead of another chromium position. The family of Cr^{3+} centers with $|b_2^0| \approx 0.0215\ \mathrm{cm}^{-1}$ was found in stoichiometric LN doped with 1 wt % of chromium.[14] Detailed investigations of angular dependencies of the EPR and ENDOR spectra, and optical absorption allowed to conclude that Cr in this center substitutes for Nb and has in the nearest surrounding the $^1H^+$ or additional Li^+ ions in structural vacancies Li_v^+ for the charge compensation. The members of the family of Cr_{Nb} centers differ from each other by the location of one or both these compensating defects.

In order to have direct evidence for the Cr^{3+} location in the centers with $|b_2^0| \approx 0.39\ \mathrm{cm}^{-1}$ and to get detailed information about the impurity surroundings, a full ENDOR investigation of these centers in LN was carried out. The parameters of hyperfine and quadrupole interactions with several nuclear shells were determined. This allowed us to find the exact chromium position (shifted from Li site). The models of chromium centers, which are able to explain all experimental data of the EPR and ENDOR are suggested.

II. CRYSTALS, EQUIPMENT, COMPUTER PROGRAMS

Special series of samples, grown by the Czochralski method from melts with different chromium concentrations (0.002–1.0 wt %) and different $x_{\mathrm{Crystal}} = ([\mathrm{Li}])/([\mathrm{Li}] + [\mathrm{Nb}])$ ratios (47.0, 48.5, 49.5, 49.85, and about 50.0%, see Refs. 5, 14–16 for details) were used.

Most of the EPR and ENDOR measurements were carried out in the temperature range 4.2–300 K at *X*-band on a Bruker ESR-200 D-SRC with ESP 360 digitally computed excitation (DICE) ENDOR system at the University of Osnabrück and on a Bruker ESR-300 spectrometer at Giessen University. Some testing *Q* and *X* band EPR investigation were performed by means of RE-1301, RE-1308 spectrometers at Institute for Problems of Material Sciences (Kiev, Ukraine). Optical absorption spectra were measured using a Bruins Instruments Omega 10/20 spectrometer.

The treatment of the EPR/ENDOR spectra (filtering, peak picking, simulations, spectra subtraction, etc.) and their angular dependencies were carried out with the help of the ''Visual EPR'' and ''Visual ENDOR'' program packages.[17] The relevant spin-Hamiltonian parameters of the paramagnetic centers were determined by a fitting procedure, based on the exact diagonalization of the corresponding matrices.

III. THEORETICAL BACKGROUND

A. LN lattice and possible surroundings of impurity centers

The ideal LN lattice (see Fig. 1 in Ref. 5) has the space group symmetry $R3c$ at room temperature[18–21] with two

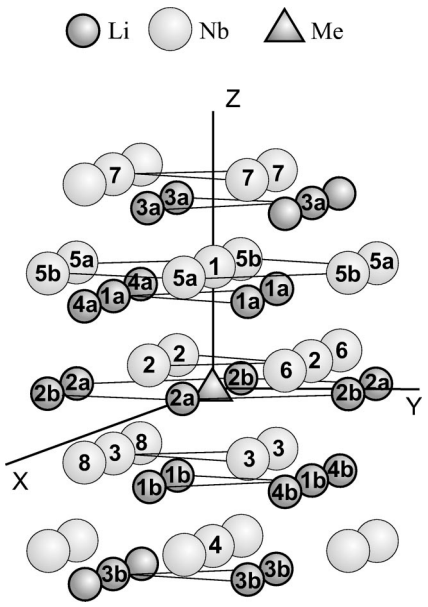

FIG. 1. Assignments of nuclear shells around the lithium site.

$LiNbO_3$ molecules in its rhombohedral elementary unit cell. All sites along the **z** (or optical **c**) axis of the crystal, including the sites of Li, Nb and the octahedral structural vacancy v, have the symmetry of the point group C_3. An isolated defect in any of these positions creates a C_3 (later on also labeled ''axial'') center. A glide mirror plane is the symmetry element, which transforms one of the two molecules into another one, and correspondingly, the surroundings of the ''right'' (*R*) center into the surroundings of the ''left'' (*L*) one. However, each of these C_3 centers has no mirror plane symmetry. Therefore, six nuclei of some shells are generally nonequivalent, although they are located at the same distance from the impurity ion (see, for instance, the shells 2a, 2b and 5a, 5b on Fig. 1 and in Table I). All other positions (oxygen site, tetrahedral vacancy, etc.) or complexes of two defects (except when both are located on the crystal **z** axis) have the lowest possible symmetry, C_1.

B. Spin Hamiltonians

The usual spin Hamiltonian, which describes the field positions of the EPR lines of centers with the spin $S = 3/2$ and arbitrary symmetry, can be written as

$$H_{\mathrm{EPR}} = \beta \mathbf{B} \cdot \mathbf{g} \cdot \mathbf{S} + \sum_q \left(b_2^q O_2^q + c_2^q \Omega_2^q \right), \quad -2 \leqslant q \leqslant 2. \quad (1)$$

Here β is the Bohr magneton, **B** is the vector of static magnetic field, **g** is the *g* tensor, **S** is the total electron spin of the paramagnetic center, b_2^q, c_2^q are the parameters of crystal field; $O_2^q = O_2^q/3$, $\Omega_2^q = \Omega_2^q/3$; O_2^q, Ω_2^q are irreducible tensor operators of electron spin, which are defined elsewhere.[22] For C_3 symmetry the spin Hamiltonian has only diagonal components of the *g* tensor and one crystal-field term having $q = 0$.

The ENDOR frequencies are described by the addition to H_{EPR} the spin Hamiltonian for *i*th nucleus,[23–25]

TABLE I. Nucleus positions and dipole-dipole interactions for the paramagnetic defect on the Li site. α and β are the azimuthal and polar angles, respectively, of the ''defect-nucleus'' direction.

Nucleus	Shell	Symmetry	Number of nuclei	Distance (Å)	Projection on c axis (Å)	b_{dd} (MHz)	α (deg)	β (deg)	Comment
Li	$1a$	C_1	3	3.765	2.31	0.576	30, 150, 270	52.15	[a]
Li	$1b$	C_1	3	3.765	−2.31	0.576	−30, 90, 210	−52.15	[a,b]
Li	$2a$, $2b$	C_1	3+3	5.149	0	0.225	0, 60, ..., 300	90	
Li	$3a$	C_1	3	5.494	4.62	0.185	−30, 90, 210	32.80	[a]
Li	$3b$	C_1	3	5.494	−4.62	0.185	30, 150, 270	32.80	[a,b]
Li	$4a$	C_1	3	6.378	2.31	0.118	−30, 90, 210	68.77	[a]
Li	$4b$	C_1	3	6.378	−2.31	0.118	30, 150, 270	−68.77	[a,b]
Li	5	C_3	1	6.932	6.932	0.092	0	0	
Nb	1	C_3	1	3.009	3.009	0.712	0	0	
Nb	2	C_1	3	3.053	0.70	0.682	−30, 90, 210	76.77	
Nb	3	C_1	3	3.381	−1.61	0.503	30, 150, 270	−61.53	[b]
Nb	4	C_3	1	3.922	3.922	0.322	0	0	
Nb	$5a$, $5b$	C_1	3+3	5.963	1.61	0.124	0,60, ..., 300	59.69	

[a]The lines of **a** and **b** shells of these nuclei are split, if the defect shifts off the normal lattice position.
[b]The nuclei of the shell were not indicated previously (Ref. 29), because the upper part of crystal lattice was considered.

$$H_i = -g_n^i \beta_n \mathbf{B}\cdot\mathbf{S} + \mathbf{S}\cdot\mathbf{A}^i\cdot\mathbf{I}^i + \mathbf{I}^i\cdot\mathbf{Q}^i\cdot\mathbf{I}^I. \quad (2)$$

β_n is the nuclear magneton, g_n is the nuclear g factor, **A**, **Q** are the tensors of hyperfine and quadrupole interactions. Relations between Cartesian A_{pq}, Q_{pq} and irreducible A_2^q, Q_2^q components of second-rank tensors are given in the literature (see Ref. 17). For systems with a large anisotropy of both Zeeman and hyperfine interactions or with $S>1/2$ (like in our case) the use of orthogonal irreducible tensors instead of nonorthogonal Cartesian tensors has indisputable advantages, since it strongly facilitates a fitting of angular dependencies of complex EPR/ENDOR spectra. All parameters of the nuclear spin Hamiltonians for L and R centers have the same absolute values, but $A_2^1(L) = -A_2^1(R)$, $A_2^{-2}(L) = -A_2^{-2}(R)$, $Q_2^1(L) = -Q_2^1(R)$, $Q_2^{-2}(L) = -Q_2^{-2}(R)$ for irreducible tensors. The procedure of the ENDOR frequencies calculations for each electron spin state M and detailed analysis of the ENDOR line multiplication caused by the shift of an impurity ion along **z** axis, by the lattice distortion, by the systematical presence of extrinsic ion or vacancy of regular ions in the surroundings were described in Ref. 14.

IV. DEPENDENCE OF THE ENDOR SPECTRA ON THE CRYSTAL COMPOSITION x_C AND CHROMIUM CONCENTRATION: PARASITIC LINES

For each sample investigated the conditions for observation of the ENDOR signals were optimized by variation of microwave and radio frequency power, time constant, modulation amplitude of radio frequency field, and number of averaging scans. The best spectra were found at liquid helium temperature (typical examples are represented in Figs. 2 and 3). Signal intensities decrease with increasing temperature and practically disappear above 50 K.

Several dozens of lines were registered between 1 and 20 MHz and four triplets between 20 and 80 MHz. The narrowest ENDOR line, which was observed in LN:Cr, had a peak-to-peak linewidth of about 0.1 MHz all other lines were broader. In crystals with high x_C the ENDOR lines were 1.5–2 times narrower than in congruent ones, however, this narrowing was not so pronounced as for EPR lines (five or more times). No essential dependence of the ENDOR linewidth on chromium concentration was found for [Cr] between 0.02 and 1 wt %.

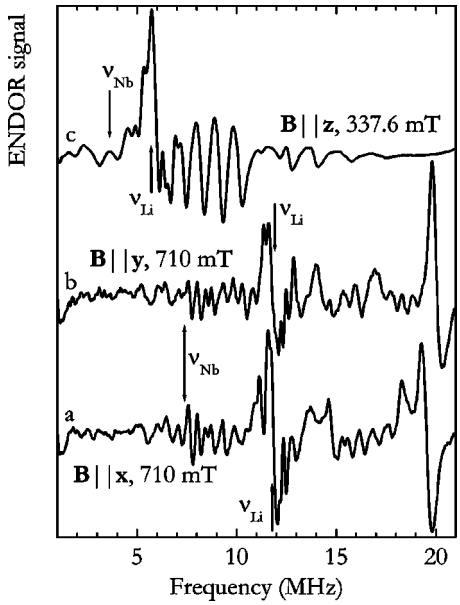

FIG. 2. Fragments of the ENDOR spectra of Cr_1^{3+} center in $LiNbO_3$ at $T=4.2$ K for samples with $x_C=49.5\%$ and [Cr] $=0.05$ wt %. The spectra were averaged out at eight scans to increase signal-to-noise ratio.

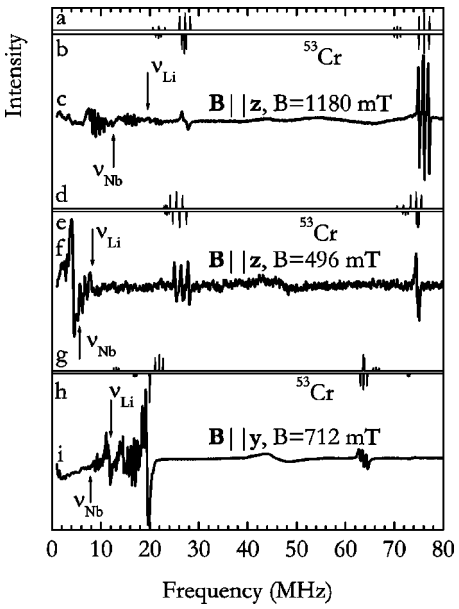

FIG. 3. The ENDOR spectra of Cr_1^{3+} in Ln, $T=4.2$ K. Simulated lines for own ^{53}Cr nucleus and for $b_2^0>0$ (a, d, g) and $b_2^0<0$ (b, e, h) are shown above experimental spectra (c, f, i) for the crystal with $x_C=49.5\%$ and $[Cr]=0.05$ wt %.

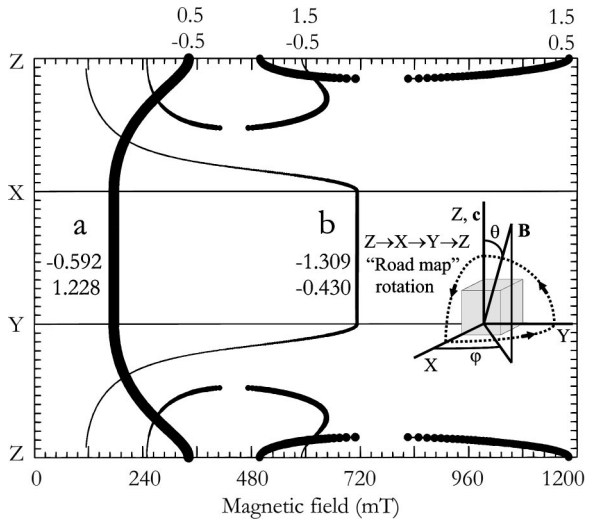

FIG. 4. Calculated angular dependence of EPR lines for Cr^{3+} center with $b_2^0=-0.387$ cm^{-1} in **z-x**, **x-y**, and **y-z** planes (road map). The sizes of symbols are proportional to the line intensities. Central (a) and high-field (b) EPR transitions and quantum numbers $\langle M|\mathbf{S}_B|M\rangle$ are indicated.

Relative intensities of different lines and line groups changed strongly (up to several times) with x_C and [Cr] due to the variation of ratios of spin-lattice and spin-spin relaxation rates. The ratio of the ENDOR signal intensities of the main axial center and the satellite centers[5] were approximately proportional to the intensities of their EPR lines: it was larger in crystals with small concentrations of intrinsic defects.

Several further signals were registered in our ENDOR measurements. Some of the signals are replicas of the ^{53}Cr lines, the strongest lines in the spectra. They were observed at the frequencies $\nu_{Cr}/2$, $\nu_{Cr}/3$, and $\nu_{Cr}/4$, where ν_{Cr} is a frequency of the ENDOR transition at arbitrary orientation of magnetic field. These lines were easily recognized, since their positions can be predicted by simple calculation. Similar replicas were registered also for the strongest ^{93}Nb lines at $\nu_{Nb}/3$, however, signals at $\nu_{Nb}/2$ and $\nu_{Nb}/4$ were practically absent. These lines probably appear because the standard Bruker radio frequency generator is not quite monochromatic.

Another unusual set of unknown signals was observed in some samples only. Their intensities were sometimes comparable with the intensities of the main ENDOR lines. The distances between lines of the set were always constant and equal to 2.1 MHz. The signals are obviously not of ENDOR type, since first, the positions of these lines do not depend on the value and orientation of magnetic field, and second, their intensities do not follow EPR signal intensities. Samples, which do not give parasitic lines, were used for the most important experiments; otherwise these lines were simply ignored at the interpretation of the ENDOR spectra.

V. ANGULAR DEPENDENCIES OF ENDOR SPECTRA

Full determination of hyperfine and quadrupole tensors with C_1 symmetry requires measurements of angular dependencies of ENDOR spectra (road map) in three orthogonal planes. A quick glance at the angular dependencies of the EPR spectra of the axial Cr_1^{3+} center (Fig. 4) shows that intensities of all transitions, except the central one, strongly depend on magnetic-field orientation. Since the ENDOR signals amount to a few percent of the EPR signal, it is possible to measure only fragments of the ENDOR angular dependencies in the **x-z** and **z-y** planes (about 15–25°) for most of the transitions. The high-field EPR transition at 712 mT gives us an opportunity for a complete investigation in the **x-y** plane. Full angular dependencies in three planes can be obtained for the central EPR transition only. Due to the low resonance magnetic fields for this transition (170–340 mT) the difference between the Li and Nb Larmor frequencies is rather small; that complicates the interpretation of observed spectra. The necessity to measure at different magnetic fields during the rotation in the **x-z** and **z-y** planes leads to angular dependencies of Larmor frequencies; that also creates certain inconveniences.

Since an unavoidable overlapping of large number of rather broad lines hampered the line tracing, very small steps of about 1° were chosen for the study of the angular dependencies. Although the ENDOR signals at the wings of the EPR line were comparable with the signal at the center of this line, during the measurements of angular dependencies the magnetic field corresponding to the center of the EPR line was mainly used. This allowed us to decrease a possible contribution of satellite centers to the ENDOR signal. Typical fragments of these dependencies are shown in Figs. 5–8. It is seen that they are very rich and very complex. To understand all details of the spectra and make their interpretation more reliable, we carried out the same measurements on four samples with different x_C and chromium concentration using two different ENDOR spectrometers (at Giessen and Osnabrück). In spite of very different ratios of relative intensities observed for some lines and line groups, the main fea-

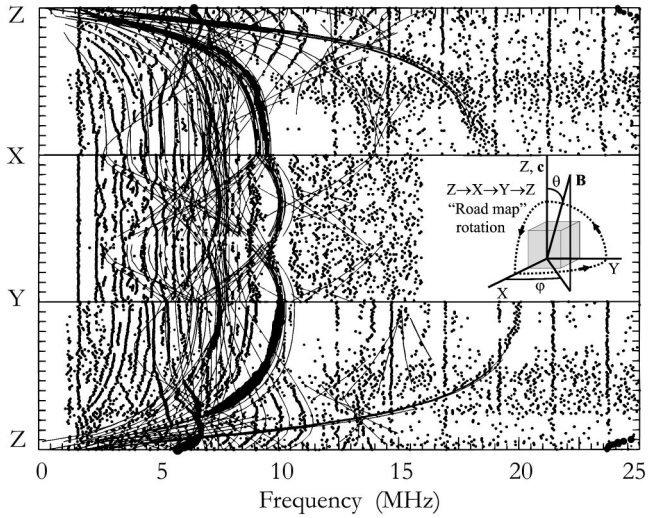

FIG. 5. Road map of the observed ENDOR signals of Cr^{3+} center for the central EPR transition. Symbol sizes reflect line intensities. Curves represent the calculated angular dependencies for the first shell of ^{93}Nb nuclei.

tures of all angular dependences obtained were practically identical. However, the investigation of these additional samples gave us decisive information for some line groups. For instance, some lines of ^{93}Nb shells were more pronounced in crystals with $x_C = 49.5\%$ than in congruent ones.

A. Lines of ^{53}Cr

Only 9.5% of the chromium ions have a nonzero magnetic moment: the isotope ^{53}Cr has $I = 3/2$ and $g_n = -0.3147$, quadrupole moment $Q = -0.028|e| \times 10^{-24}$ cm^2. It is comparatively easy to find and to trace their triplets in the ENDOR spectra—they have the largest frequencies and sometimes the highest intensities (Fig. 3). Although each EPR line corresponds to the transition between two electron spin states (except of the rare directions of magnetic field, where an

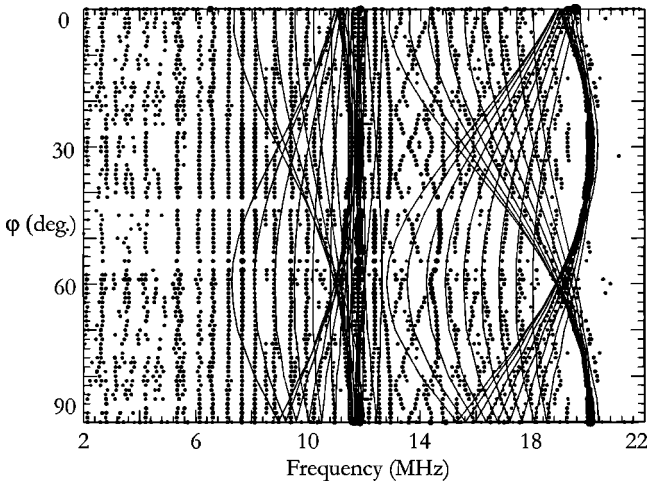

FIG. 6. Observed ENDOR signals of Cr^{3+} center for high-field EPR transition in **x**-**y** plane (symbols). Lines, calculated angular dependencies for the first shell of ^{93}Nb nuclei.

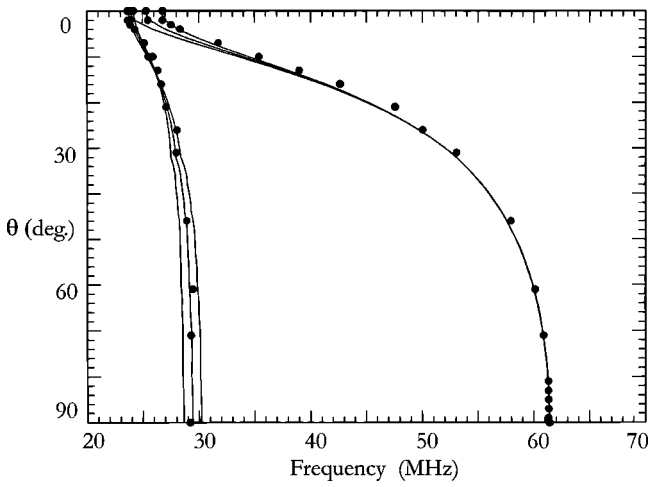

FIG. 7. Observed (symbols) and calculated (lines) ENDOR signals for own ^{53}Cr nucleus of Cr^{3+} center for central EPR transition in **z**-**x** plane in congruent crystal.

overlapping of two EPR lines takes place), in the ENDOR spectra of LN:Cr the four triplets, which belong to all four electron spin states, were observed very often. This overcrowds the spectra, however, sometimes it facilitates their evaluation.

The spectra in Fig. 3 show that quadrupole splitting is different for different M. It can be explained only if contributions of $(H_i)^2/H_{\mathrm{EPR}}$ are taken into account. Since this effect depends on the relative signs of the parameters of the spin Hamiltonians (1) and (2), it becomes possible to determine them from the comparison of calculated and observed ENDOR frequencies (the positions of EPR lines depend only on $|b_2^0|$). The analysis of the quadrupole splitting for $\mathbf{B} \| \mathbf{z}$ and $\mathbf{B} \perp \mathbf{z}$ confirms the conclusion[11] that the parameter of isotro-

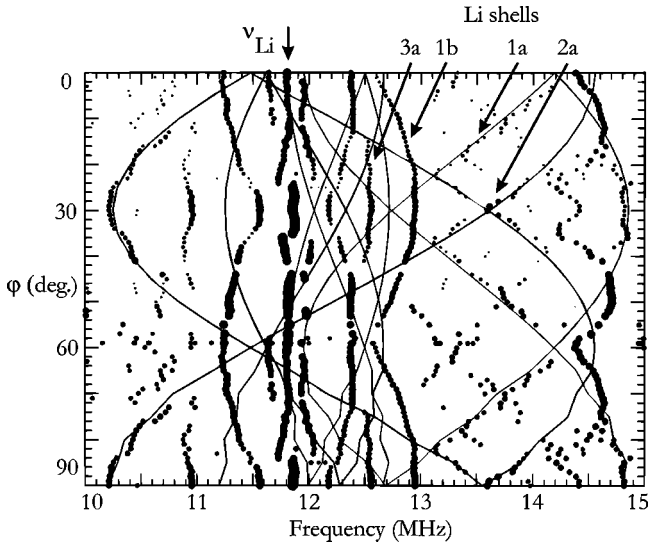

FIG. 8. Fragment of observed ENDOR signals (symbols) of Cr^{3+} center for high-field EPR transition in **x**-**y** plane for the crystal with $x_C = 49.5\%$ and $[\mathrm{Cr}] = 0.05$ wt %. Lines, calculated angular dependencies for ^{7}Li nuclei of $1a$ (thin lines) and $2a$ (thick lines) shells.

TABLE II. Comparison of characteristics of crystal field, hyperfine and quadrupole interactions with the ^{53}Cr nucleus for different Cr^{3+} centers.

	Center, crystal			
Parameter	Axial Cr_{Li} $LiNbO_3$, $T=4.2$ K (this work)	Axial Cr_{Nb} $LiNbO_3$, $T=4.2$ K (Ref. 14)	Cr_{Nb} $LiNbO_3$:Mg (Refs. 12, 13)	Axial Cr_{Al} Al_2O_3 (Ref. 38)
g	1.97	1.995	1.971	1.99
b_2^0 (cm^{-1})	-0.387	± 0.0215	<0.01	-0.191
$a=A_0^0=(A_{xx}+A_{yy}+A_{zz})/3$ (MHz)	49.5	50.97	50.93	48.5
$b=A_2^0=(2A_{zz}-A_{xx}-A_{yy})/6$ (MHz)	-0.3	-0.13	-0.066	0
Q_2^0 (MHz)	-0.32	0.14	0.1	-0.21
a/gg_n (MHz)	-79.8	-81.2	-82.1	-77.4

pic (contact) hyperfine interaction a for Cr_1^{3+} is positive, whereas parameters of axial crystal field b_2^0 and quadrupole interaction Q_2^0 are negative (Table II). Although the hyperfine interaction is expected to be nearly isotropic and the magnetic moment of ^{53}Cr is rather small, it was observed that during rotation of magnetic field in the **z**-**x** and **z**-**y** planes the chromium triplets move surprisingly from 62 to 26 MHz (Fig. 7). A computer simulation of ENDOR spectra has shown that this effect is caused by the very strong change of matrix elements $\langle M|\mathbf{S}|M\rangle$. Since for the Cr_1^{3+} center the axial crystal field splitting of about 0.8 cm^{-1} is comparable with the Zeeman splitting for magnetic fields of about 100–1000 mT, the values of $\langle M|\mathbf{S}_B|M\rangle$ strongly deviate from $\pm 3/2$, $\pm 1/2$, which are typical for high magnetic fields (see Fig. 4). The fitting of the experimental angular dependencies gave $a=49.5$ MHz and parameter of anisotropic HFI $b=-0.3$ MHz.

B. Lines of ^{93}Nb shells

It is easy to recognize the ENDOR lines of the ^{93}Nb nucleus ($I=9/2$, natural abundance 100%, $g_n=1.3712$, $Q=-0.28$ $|e|\times 10^{-24}$ cm^2) due to the characteristic multiplets of nine lines with the intensity ratios 9:16:21:24:25:24:21:16:9. It is much more difficult to trace such multiplets, when they are overlapped. We managed to trace several shells of Nb nuclei and to determine their parameters by fitting. Figures 5 and 6 show comparison of calculated and observed angular dependencies. The obtained parameters of hyperfine interactions for low-symmetry shells (Table III) are unexpectedly very high. They are several times larger than the predicted dipole-dipole interactions.

The extrema of the angular dependencies of the ENDOR frequencies in the **x**-**y** plane occur near the angles 0°, 30°, 60°, and 90°. These directions correspond to the projections of the radius vector $\mathbf{R}^i$ from an impurity ion to regular lattice sites of nearest cation shells onto **x**-**y** plane.

We paid special attention to search for lines without angular dependence in the **x**-**y** plane, nuclei on the center axis should give such lines. The only group of Nb lines, which we found, has a very small hyperfine interaction and a parameter of axial quadrupole interaction $Q_2^0 \approx 0.55$ MHz. The parameter Q_2^0 is related to the value eqQ, which is usually used in

TABLE III. Parameters of hyperfine and quadrupole interactions of the Cr^{3+} center in lithium niobate.

	Hyperfine interaction (MHz)			Euler angles for rotation from **x**, **y**, **z** to 1, 2, 3 axes (deg)			Quadrupole interaction (MHz)		Euler angles for rotation from **x**, **y**, **z** to 1, 2, 3, axes (deg)			Shell no.	a/gg_n (MHz)
Nucleus	a	b	b'	α_A	β_A	γ_A	Q_2^0	Q_2^2	α_Q	β_Q	γ_Q		
Nb	7.66	1.014	-0.476	90	85	90	0.48	-0.176	90	29	270	2	2.836
Nb	4.64	0.889	-0.859	90	40	0	0.856	-0.196	90	6	0	3	1.72
Nb	2.77	0.947	-0.292	309	8	192	0.63	-0.42	19	-57	77	5a, b or 3 for Cr_2	1.026
Li	1.06	1.446	-0.226	90	53	180	<0.05					1a	0.248
Li	0.65	1.084	-0.034	90	38	0	<0.05					1b	0.151
Li	0.4	0.875	-0.739	0	90	78	<0.05					2a or 2b	0.082
Li	0.25	1.05	-1.07	0	90	95.4	<0.05					2b or 2a	0.058
Li	0.25	0	-0.4	0	0	0	<0.05					3 or 4	0.058

Here $a=(A_{11}+A_{22}+A_{33})/3$, $b=(2A_{33}-A_{11}-A_{22})/6$, $b'=(A_{11}-A_{22})/2$, $Q_2^0=3Q_{33}/2$, $Q_2^2=3(Q_{11}-Q_{22})/2$; A_{ii} and Q_{ii} ($i=1,2,3$) are the principal values of hyperfine and quadrupole tensors, respectively.

nuclear magnetic resonance (NMR), by the expression $Q_2^0 = 3\ eqQ/4I(2I\text{-}1)$. Based on $|eqQ| = 22-23.6$ MHz from NMR data[26] for Nb nuclei in the bulk of the crystal, we estimated that $Q_2^0(\text{bulk}) = 0.51-0.55$ MHz. Since both HFI and Q_2^0 for this registered group of Nb lines are very close to the bulk values, we are inclined to suppose that these lines rather belong to distant nuclei than to nuclei on the center axis.

The interpretation of the dependencies for **z**-**x** and **z**-**y** planes is more complicated, since they are results of competitive angular dependencies of Larmor frequency, $\langle M|\mathbf{S}|M\rangle$, HFI and quadrupole interaction.

C. Lines of ^{7}Li shells

The main isotope ^{7}Li has $I = 3/2$, a natural abundance 92.5%, $g_n = 2.170\,96$, and a quadrupole moment $Q = -0.040|e| \times 10^{-24}$ cm^2. The quadrupole splitting for distant nuclei, estimated on the basis of NMR data[27] should be about 0.014 MHz. Since the observed lines have widths of about 0.1 MHz, such a splitting cannot be resolved. Even if the electric field gradient near to the chromium ion is several times larger than in the bulk, the quadrupole triplet of ^{7}Li will merge into a single line. We found several shells with such lines near to Larmor frequency of ^{7}Li (see Fig. 8). The obtained parameters of the hyperfine interactions (Table III) are again larger than the predicted dipole-dipole interactions.

Although some low-intensity single lines without angular dependence in the *x*-*y* plane could be indicated in the measured spectra, their partners from another electron spin state were not found; therefore we have no reliable interpretation of these lines (we cannot exclude even that their angular independence is a fruit of our imagination, since a lot of much more intense lines move through the investigated region of frequencies).

D. Search for lines of other nuclei

Unintended trace impurities (C, Cu, Fe, Co, Ta,...) are always present in LN. Since the chromium concentrations of studied samples are one or two order larger than the concentrations of these noncontrolled impurities (about $0.00X$ mol %), the latter cannot be associated with each Cr^{3+} ion. However, we are obliged to consider a possibility that some of them can be present in the neighborhood of a part of chromium ions. We checked especially also the nuclei: ^{1}H, ^{19}F, ^{27}Al, ^{39}K (for the samples grown from a melt with an addition of potassium), ^{53}Cr from ions in 2+ or 4+ states (they do not reveal themselves in EPR). No lines belonging to these nuclei were found. This means that the Cr_1^{3+} center can have in its surroundings only the Li, Nb, their vacancies and, theoretically, the ''ENDOR silent'' foreign ions (ions with nuclei without magnetic moments).

VI. ENDOR SPECTRA OF SATELLITE CENTERS

Satellite chromium centers $Cr_2^{3+}\cdots Cr_9^{3+}$ have a nature common with the main Cr_1^{3+} center.[5] Since angular dependencies of their EPR lines are rather complex at this step we investigated their ENDOR spectra at special directions only. Figure 9 represents the ENDOR signal for different values of permanent magnetic field at **B**$\|$**y**. The field of about 712 mT corresponds to one of the EPR transitions of Cr_1^{3+} centers (see Fig. 4), all other values—to the same transition of satellite centers. Since the EPR line intensities for satellite centers are essentially lower than for the main center, their ENDOR signals have also lower intensities. Nevertheless, for satellite lines with resonance fields of about 626 and 792 mT the appearance of additional groups of Nb lines with frequencies 19–22 MHz ($a \approx 9-10$ MHz) was found. These lines have parameters of HFI and quadrupole interactions, which are larger than for the Cr_1^{3+} center. The observed redistribution of electron density and electric field gradients indicates that some defect with a strong perturbation is present in the nearest neighborhood of this kind of satellite centers. Since lines of other nuclei, except Cr, Li, and Nb, were not found, this defect can be a vacancy, an ''ENDOR silent'' ion, or a nonregular Li or Nb. For instance, a lack of one of the six Nb^{5+} ions in chromium surrounding can cause an essential increase of electron densities on other positively charged ions.

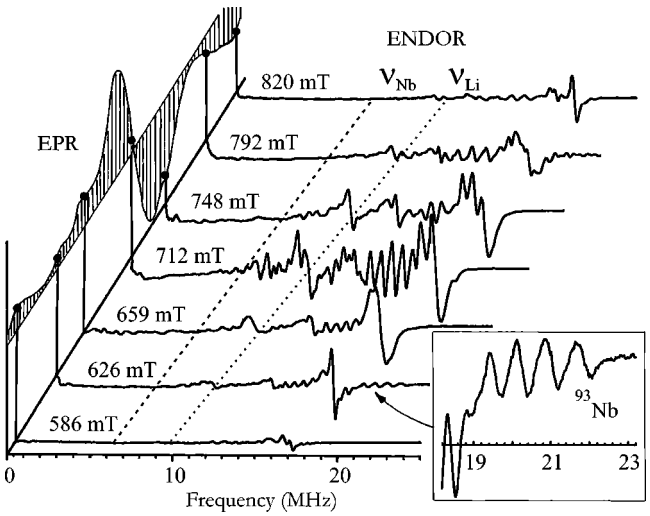

FIG. 9. Observed ENDOR signals for different parts of overlapping EPR lines of the Cr_1^{3+} and satellite centers in LN. **B**$\|$**y**, $\nu = 9.4$ GHz, $T = 4.2$ K, $x_C = 49.5\%$, and [Cr] = 0.05 wt %.

A strong increase of HFI could take place also for the chromium incorporation in a tetrahedral vacancy due to closer location of the nearest Nb nuclei (about 1.72 Å). However, characteristics of crystal fields for this low-symmetry center with tetrahedral surrounding should be quite differ from observed b_2^0 parameters for Cr_{Li} centers within oxygen octahedron.

VII. RECONSTRUCTION OF EPR LINE ON THE BASIS OF ENDOR DATA

To check the self-consistence of the determined HFI parameters we have to reconstruct the shape of the EPR line. If we suppose that the hyperfine interactions are close to dipole-dipole ones, the predicted inhomogeneous broadening of the EPR lines should be about 0.3–0.5 mT, whereas the

measured linewidths for conventional LN crystals are about one or two orders larger. Despite the availability of some ENDOR data[12,24,28,29] this drastic contradiction was not discussed previously, since conventional congruent crystals and even Li-rich crystals used for these measurements have usually a lot of intrinsic defects. Therefore the difference between the calculated and observed linewidth could be ascribed to these defects. Recently, several ways were developed to obtain perfect crystals with $x_C \approx 50.0\%$ (growth from the melt with an addition of potassium,[15,30–33] double crucible growth,[34,35] postgrowth vapor transport equilibration treatment[36–38]). These crystals have extremely low concentrations of intrinsic defects, and the ascription mentioned above is not valid anymore. In all cases when the linewidth of the observed EPR line is much greater than the linewidth reconstructed on the basis of the ENDOR data, we have to clarify reasons of this contradiction (nonperfect crystals, nonoptimal condition for the measurements, lost ENDOR lines, unreliable evaluations, nonsatisfactory interpretation,...) and have to eliminate sources of possible errors.

The shape and width of the observed EPR lines in LN strongly depends on many parameters: crystal composition, chromium concentration, magnetic-field direction, and temperature. The line of the central EPR transition usually is narrower than those of the other transitions. In order to carry out a reliable comparison of simulated and experimental spectra we investigated the line of the central EPR transition at $\mathbf{B} \| \mathbf{z}$, at 4.2 K for a crystal with x_C of about 50.0% and rather low chromium concentration (0.02 wt %). Under these conditions the effects of all mechanisms of line broadening described above are essentially reduced and we can assume that hyperfine interactions give dominating contributions to the EPR linewidth (inhomogeneous broadening). For simulation of the EPR spectrum we used two approaches: a reconstruction with the help of the algorithm described in Ref. 24, and the straightforward calculation of EPR spectra of many nuclear systems. Both methods gave similar results. A good agreement of lines calculated on the basis of our ENDOR data (Table III) and experimental ones (Fig. 10) gives evidence of the correctness of the evaluation and interpretation of our complex ENDOR spectra. We have to conclude also that the Nb nucleus of the first shell not found in our ENDOR investigation (if it is present at all) should have a HFI much smaller than the HFI of the second or third shells, otherwise the simulated EPR line becomes broader than the observed one.

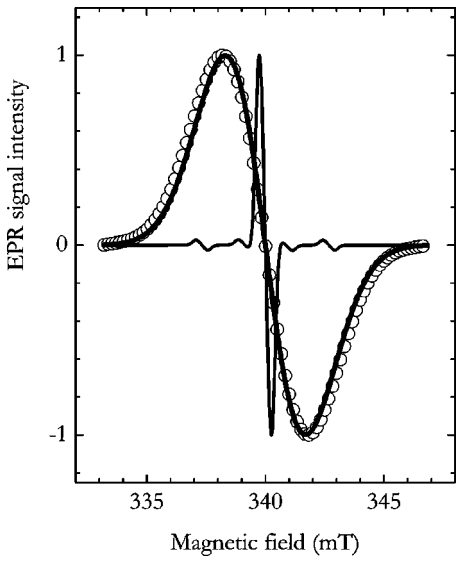

FIG. 10. Reconstruction of line shape of the central EPR transition on the basis of ENDOR data. Circles, experimental EPR line measured for LN crystal with x_C about 50.0% and 0.02 wt % Cr at $\mathbf{B} \| \mathbf{z}$, $\nu = 9.4$ GHz, and $T = 4.2$ K. The solid lines were calculated with the help of hyperfine parameters listed in Table III (thick lines) and with the parameters of dipole-dipole interactions from Table I (thin lines).

VIII. STRUCTURE OF THE Cr_1^{3+} CENTER

According to the simplest theory the parameter of the isotropic (contact) HFI of paramagnetic electrons with ith nucleus

$$a^i \equiv A_0^{0,i} = Sp\mathbf{A}^i/3 = 8\pi g\beta g_n^i \beta_n |\psi(\mathbf{R}^i)|^2/3, \qquad (3)$$

where $|\psi(\mathbf{R}^i)|^2$ is the electron density in the point $\mathbf{R}^i$ of nucleus location. Based on the measured parameters of HFI (Table III), we found that for Cr_1^{3+} center the values of electron density on Nb nuclei are essentially higher than on Li nuclei. This can be easily explained if the chromium ion substitutes Li or occupies an octahedral vacancy site and has Nb nuclei in the nearest cation neighborhood. In the case of Nb substitution the nearest cation surroundings are Li nuclei, and hyperfine interactions with these nuclei should be the strongest ones.

Very often (for instance, at distances so large that the interacting magnetic moments can be considered as point dipoles) the anisotropic part of the HFI has to be close to the classical dipole-dipole interaction. The axis of the dipole-dipole interaction of the impurity with ith nucleus has to coincide with the direction of $\mathbf{R}^i$, and the value of b_{dd}^i can be estimated with the help of the expression

$$b_{dd}^i = 14.17 g_n^i / [R^i(\text{Å})]^3 \ \text{MHz}.$$

Anisotropic parts b^i of HFI observed for the Cr_1^{3+} center are larger than the b_{dd}^i calculated for Li and Nb substitution (Table 1 and Table 3 in Ref. 14) as well as for the vacancy occupation. Nevertheless, since for the nearest shells the extrema of the angular dependencies of the ENDOR frequencies in the **x-y** plane coincide with the projections of $\mathbf{R}^i$ onto the **x-y** plane for cations (azimuthal angles 0, 30, 60, and 90°), we may suppose that one of the axes of the low-symmetry HFI is very close to $\mathbf{R}^i$, i.e., that polar angle of this axis is close to the polar angle of the $\mathbf{R}^i$ vector. Then, assuming that the surrounding ions are located at regular lattice sites, we can compare the principal directions of HFI tensors for possible center models. Figure 11 shows that the principal directions of the second and third shells of Nb nuclei have a common point only in the case of Li substitution, and that this point is not exactly the regular Li site. Therefore

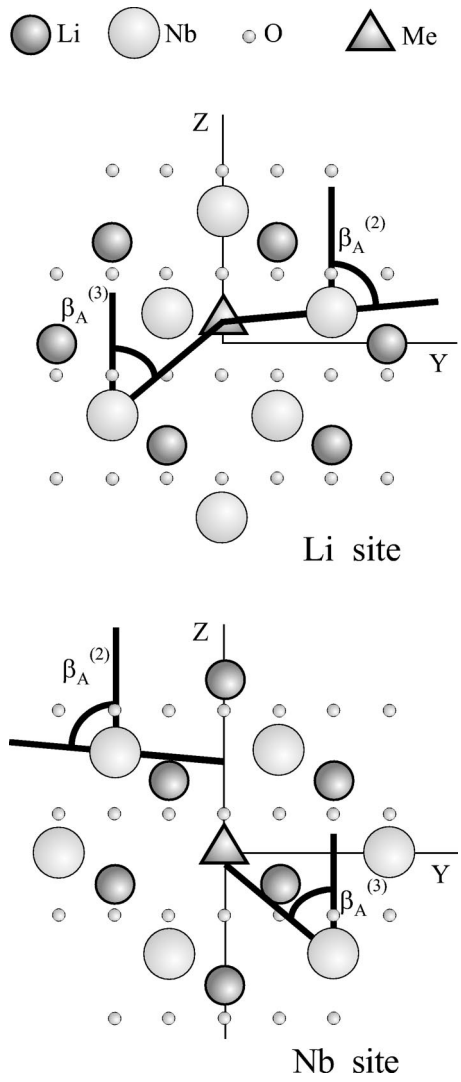

FIG. 11. Comparison of principal directions of hyperfine tensors for the case of Li and Nb substitutions (the projection on **z**-**y** plane) and estimation of a possible shift of the chromium ion from regular Li site. $\beta_A^{(2)}$, $\beta_A^{(3)}$ are the β_A angles for the second and third Nb shells, respectively, from Table III.

we can conclude that for Cr_1^{3+} center the Li substitution is realized, and that the chromium ion is shifted by about 0.2 Å from the Li site.

We have to mention that the correspondence of the principal directions and the $\mathbf{R}^i$ vectors is not valid for quadrupole tensors. Since lattice ions in LN are located in noncubic positions, nonzero electric field gradients on nuclei exist even in an ideal crystal. The impurity ion creates additional gradients, which are comparable (near to the impurity ion) or much smaller (at large distances from the impurity) than gradients of crystal-lattice ions.

Comparing the principal directions of other HFI tensors with the $\mathbf{R}^i$ vectors of lattice ions we can determine the relations between the measured parameters and shells of various nuclei. We found this correspondence for the Cr_{Li} model (Table III), however, we met many difficulties if the occupation of Nb site or structural vacancy is supposed.

With the help of Eq. (3) we calculated the distribution of electron spin density a^i/gg_n^i (Tables II and III). It is negative (about -80 MHz) for the own ^{53}Cr nucleus. Since electron density of $3d$ electrons is equal to zero at the own nucleus, the origin of nonzero negative density is a polarization of $1s$, $2s$, and $3s$ core electrons by $3d$ electrons. The spin densities for surrounding nuclei are unexpectedly rather high. They are positive and decrease with increasing distance from the chromium ion. The densities at Nb nuclei are several times larger than on the Li ones; this is obviously related to the stronger attraction of chromium electrons to the larger positive charge of Nb^{5+}.

Our ENDOR data do not give an obvious evidence for the presence of another defect (or defects) in the neighborhood of the main axial Cr_1^{3+} center. The found shift of the chromium ion from the Li site can be explained by the nonisovalent replacement. The lack of ENDOR lines from the nearest Nb nucleus on the center axis can be caused by an absence of this ion. However, they could be also unobservable, if conditions for their observation are nonoptimal or if HFI parameters are very small (nodal line for $3d^3$ wave function).

IX. STRUCTURE OF THE Cr^{3+} SATELLITE CENTERS

For low-symmetry satellite centers we have direct evidence of the presence of some defect in the nearest neighborhood. Since Cr^{3+} substituting for Li^+ has two additional positive charges, it would be very unlikely that this defect also has a positive charge (instead of a negative one for the charge compensation). Therefore, interstitial Li^+ or Nb^{5+}, antisite $Nb_{Li^+}^{5+}$ and the oxygen vacancy v_O^{2-} should be discarded, as well as noncontrolled impurities. An additional interstitial oxygen ion can give required charge compensation, therefore $Cr_{Li}^{3+}-O^{2-}$ complexes have to be considered as possible models for the axial and low-symmetry centers. However, in this case it is not easy to explain directly (in the frame of conventional schemes of LN nonstoichiometry) the observed disappearance of satellite centers,[5] a decrease of chromium incorporation and the appearance of Cr_{Nb}^{3+} centers[14] in crystals with $x_{crystal} \approx 50\%$: the concentration of $Cr_{Li}^{3+}-O^{2-}$ complexes with the local charge compensation should not depend on the concentration of Nb_{Li} and cation vacancies.

Among other intrinsic defects with relative negative charge—the antisite $Li_{Nb^{5+}}^{+}$ lithium and niobium vacancies, v_{Li}^{+} and v_{Nb}^{5+}, the Li_{Nb} and v_{Nb}^{5+} give a more logical and natural explanation of both the EPR (see Ref. 5) and the ENDOR data. All satellite centers are Cr_{Li} centers with one of these defects in the second or further niobium shells. The additional 4- or 5-charge, repelling chromium electrons, should increase the electron density (and correspondingly HFI) at the other neighboring Nb^{5+} nuclei. Just this was observed in our ENDOR study (see Sec. VI).

The main chromium center, most probably, has no such defects in its neighborhood (however, the presence of one of them in the first niobium shell on the z axis should be considered as a possible alternative). The observation of low-symmetry exchange coupled chromium pairs in nonstoichio-

metric crystals at a comparatively low Cr concentration and their disappearance in regularly ordered crystals becomes also understandable in the frame of the chosen idea: these pairs are C_1 complexes formed from one v_{Nb} (or one Li_{Nb}) and two Cr_{Li}, which are located at two nearest Li sites.

X. CONCLUSIONS

The reported detailed analysis and classification of possible surroundings of impurities in different lattice sites allows us to understand the main features of the ENDOR spectra observed and can be helpful for other paramagnetic centers. The use of crystals with different x_C and various chromium concentrations offered many advantages for the investigation of the impurity centers. It gave us an opportunity to find crystals with optimal conditions for the observation of ENDOR. It facilitated also an analysis of the spectra and simplified the interpretation of the data. For the main axial Cr_1^{3+} center a full investigation of the ENDOR spectra and their angular dependencies was carried out. The ENDOR spectra of satellite chromium centers have also been studied.

Summarizing all our results we can make the following conclusions.

In all LN crystals from congruent to nearly stoichiometric composition the chromium ion replaces Li^+ in the case of the main axial center Cr_1^{3+} as well as for satellite centers Cr_2^{3+}-Cr_9^{3+}.

Chromium ion in the Cr_1^{3+} center is shifted by 0.2 Å from the regular Li-site. The determined shift is close to the value derived on the basis of PIXE data for the Cr_{Li} center.[10]

The analysis of the quadrupole splitting of ^{53}Cr shows that the parameter of the axial crystal field is negative: $b_2^0 = -0.387\ cm^{-1}$ at 4.2 K. It is interesting to note that the signs and values of the parameters b_2^0, a, and Q_2^0 for the Cr_1^{3+} center, which needs a defect for the charge compensation (independently of Li^+ or Nb^{5+} replacement), are close to the parameters of Cr^{3+} in Al_2O_3, where chromium substitutes Al^{3+} and had no defects in its surroundings[39] (Table II). However, they differ essentially from the parameters of Cr^{3+} in Mg doped LN and Cr_{Nb}^{3+} (Ref. 14).

Determined parameters of the hyperfine interactions are several times larger than expected for pure dipole-dipole interactions. Rather high values of isotropic (contact) HFI give us the evidence for a transfer of the electron density to neighboring nuclei. The determined parameters of hyperfine and quadrupole interactions present a reliable starting point for theoretical calculations.

The strong distortion of the electron density distribution derived from the ENDOR spectra of satellite centers confirms the conclusion[5] that they have an intrinsic defect in the chromium surroundings. Models with v_{Nb} or Li_{Nb} as a charge compensator of Cr_i center are able to explain most of the details of both EPR and ENDOR spectra in a natural way.

The observed narrowing of the ENDOR lines in stoichiometric crystals is less pronounced than for the EPR lines.

The shape and width of the ENDOR lines for perfect crystals with low chromium concentration are close to the simulated ones on the base of ENDOR data. This proves the correctness of the interpretation of the ENDOR data. On the other hand that presents a good basis for the use of the difference between the calculated and observed widths of the Cr_1^{3+} EPR lines for the estimation of the imperfection of nonstoichiometric crystals.

The successful reconstruction of EPR spectra for both Cr_{Li} and Cr_{Nb} centers for crystals with decreased concentration of intrinsic defects allows us also to formulate an empirical rule: widths of EPR lines for the impurity substituting for Li are usually larger than for the same impurity substituting for Nb. In the case of Cr^{3+} the linewidths of central EPR transition are approximately equal to 3 and 1 mT, correspondingly. The unresolved superhyperfine structure for Me_{Li} centers having Nb nuclei with $I=9/2$ in the nearest neighborhood should cause essentially larger broadening of the EPR lines than the hyperfine interactions with similar number of surrounding Li nuclei ($I=3/2$) for Me_{Nb} impurities.

Obtained results, together with the determined structure of the Cr_{Nb}^{3+} centers,[14] can give a key for understanding of recent results of optical absorption, luminescence, photoexcitation, and photoluminescence spectra in chromium doped nearly stoichiometric LN crystals.[40–48] We hope that our ENDOR study presents decisive arguments for the long standing discussion (see references in Ref. 5) about the location of the chromium in Cr_1^{3+}-Cr_9^{3+} centers. It shows also a possibility and necessity to perform similar ENDOR studies for other paramagnetic centers created by transition metals and rare-earth impurities, which are of special importance for optical applications.

ACKNOWLEDGMENTS

In its various stages this work has been partly supported by grants from INTAS, BMBF, ESF, DFG (in the frame of SFB 225). It was carried out in cooperation with many scientists, and we are very grateful to all members of the Magnetic Resonance Spectroscopy Groups at the Universities of Osnabrück and Giessen.

*Email address: gmalovic@uos.de

†Email address: vgrachev@uos.de

[1] G. Burns, D. F. O'Kane, and R. S. Title, Phys. Rev. **147**, 314 (1967).

[2] N. F. Evlanova, L. S. Kornienko, L. N. Rashkovich, and A. O. Rybaltovskii, Sov. Phys. JETP **26**, 1090 (1968).

[3] A. M. Glass, J. Chem. Phys. **50**, 1501 (1969).

[4] D. J. Rexford, Y. M. Kim, and H. S. Story, J. Chem. Phys. **52**, 860 (1970).

[5] G. Malovichko, V. Grachev, E. Kokanyan, and O. Schirmer, Phys. Rev. B **59**, 9113 (1999).

[6] G. I. Malovichko, V. G. Grachev, and S. N. Lukin, Sov. Phys. Solid State **28**, 553 (1986).

[7] R. Vianden, in *Insulating Materials for Optoelectronics. New Developments*, edited by F. Agullo-Lopez (World Scientific, Singapore, 1995), p. 125.

[8] A. Kling, J. C. Soares, and M. F. da Silva, in *Insulating Materials for Optoelectronics, New Developments* (Ref. 7), p. 175.
[9] G. Corradi, A. V. Chadwick, A. R. West, K. Cruickshank, and M. Paul, Radiat. Eff. Defects Solids **134**, 219 (1995).
[10] A. Kling, J. C. Soares, M. F. da Silva, J. A. Sanz-Garsia, E. Dieguez, and F. Agullo-Lopez, Nucl. Instrum. Methods Phys. Res. B **136–138**, 426 (1998).
[11] V. G. Grachev, G. I. Malovichko, and V. V. Troitskii, Sov. Phys. Solid State **29**, 349 (1987).
[12] G. Corradi, H. Soethe, J.-M. Spaeth, and K. Polgar, J. Phys.: Condens. Matter **3**, 1901 (1991).
[13] G. Corradi, H. Söthe, J.-M. Spaeth, and K. Polgar, Ferroelectrics **125**, 295 (1992).
[14] V. Grachev and G. Malovichko, Phys. Rev. B **62**, 7779 (2000).
[15] G. I. Malovichko, V. G. Grachev, L. P. Yurchenko, V. Ya. Proshko, E. P. Kokanyan, and V. T. Gabrielyan, Phys. Status Solidi B **133**, K29 (1992).
[16] G. I. Malovichko, V. G. Grachev, and O. F. Schirmer, Solid State Commun. **89**, 195 (1994).
[17] V. G. Grachev (unpublished), all details and light version to download can be found on home page, http://www.physik.uni.osnabrueck.de/resonanz/Grachev
[18] S. C. Abrahams, J. M. Reddy, and J. L. Bernstein, J. Phys. Chem. Solids **27**, 997 (1966).
[19] S. C. Abrahams, W. C. Hamilton, and J. M. Reddy, J. Phys. Chem. Solids **27**, 1013 (1966).
[20] S. C. Abrahams, H. J. Levinstein, and J. M. Reddy, J. Phys. Chem. Solids **27**, 1019 (1966).
[21] A. Räuber, in *Current Topics in Material Sciences*, edited by E. Kaldis (North-Holland, Amsterdam, 1978), Vol. 1, p. 481.
[22] S. A. Altshuler and B. M. Kozirev, *Electron Paramagnetic Resonance in Compounds of Transition Elements* (Wiley, New York, 1974).
[23] A. Abragam and B. Bleaney, *Electron Paramagnetic Resonance of Transition Ions* (Clarendon, Oxford, 1970).
[24] M. D. Glinchuk, V. G. Grachev, M. F. Deigen, A. B. Roitzin, and L. A. Suslin, *Electric Effects in Radiospectroscopy. Electron Paramagnetic, Electron Nuclear Double and Paraelectric Resonance's* (Nauka, Moscow, 1981), pp. 1–332, in Russian.
[25] J.-M. Spaeth J. R. Niklas, and R. H. Bartram, *Structural Analysis of Point Defects in Solids: An Introduction to Multiple Magnetic Resonance Spectroscopy* (Springer, Singapore, 1992).
[26] E. Schempp, G. E. Peterson, and J. R. Carruthers, J. Chem. Phys. **53**, 306 (1970).
[27] G. E. Peterson and P. M. Bridenbaugh, J. Chem. Phys. **48**, 3402 (1968).
[28] G. Corradi, H. Soethe, J.-M. Spaeth, and K. Polgar, J. Phys.: Condens. Matter **2**, 6603 (1990).
[29] H. Soethe and J.-M. Spaeth, J. Phys.: Condens. Matter **4**, 9901 (1992).
[30] G. I. Malovichko, V. G. Grachev, E. P. Kokanyan, O. F. Schirmer, K. Betzler, B. Gather, F. Jermann, S. Klauer, U. Schlarb, and M. Wöhlecke, Appl. Phys. A: Solids Surf. **A56**, 103 (1993).
[31] A. Kling, J. G. Marques, J. G. Correia, M. F. da Silva, E. Dieguez, F. Agullo-Lopez, and J. C. Soares, Nucl. Instrum. Methods Phys. Res. B **113**, 293 (1996).
[32] V. Bermudez, P. S. Dutta, M. D. Serrano, and E. Dieguez, J. Phys.: Condens. Matter **9**, 6097 (1997).
[33] K. Polgar, A. Peter, L. Kovacs, G. Corradi, and Zs. Szaller, J. Cryst. Growth **177**, 211 (1997).
[34] N. Iyi, K. Kitamura, F. Izumi, J. K. Yamamoto, T. Hayasgi, H. Asano, and S. Kimura, J. Solid State Chem. **101**, 340 (1992).
[35] K. Kitamura, Y. Furukawa, and N. Iyi, Ferroelectrics **202**, 21 (1997).
[36] P. F. Bordui, R. G. Norwood, C. D. Bird, and G. D. Calvert, J. Cryst. Growth **113**, 61 (1991).
[37] D. H. Jundt, M. M. Fejer, and R. L. Byer, IEEE J. Quantum Electron. **26**, 135 (1990).
[38] C. Fischer, S. Kapphan, Xi-Qi Feng, and Ning Cheng, Radiat. Eff. Defects Solids **135**, 199 (1995).
[39] R. W. Terhune, J. Lambe, C. Kikuchi, and J. Baker, Phys. Rev. **123**, 1265 (1961).
[40] F. Lhomme, P. Bourson, M. D. Fontana, G. Malovichko, M. Aillerie, and E. Kokanyan, J. Phys.: Condens. Matter **10**, 1137 (1998).
[41] A. Skvortsov, V. Trepakov, S. Kapphan, V. Vorlicek, and L. Jastrabik, Radiat. Eff. Defects Solids **150**, 293 (1999).
[42] G. M. Saley, S. A. Basun, G. F. Imbusch, A. A. Kaplyanskii, S. Kapphan, R. S. Metzler, and U. Happek, J. Lumin. **83–84**, 423 (1999).
[43] S. A. Basun, G. M. Saley, A. A. Kaplyanskii, H. G. Gallagher, K. Polgar, L. Lu, and U. Happek, J. Lumin. **83–84**, 435 (1999).
[44] A. Kamin'ska, J. E. Dmochowski, A. Suchocki, J. Garcia-Sole, F. Jaque, and L. Arizmendi, Phys. Rev. B **60**, 7707 (1999).
[45] A. Kamin'ska, A. Suchocki, L. Arizmendi, D. Callejo, F. Jaque, and M. Grinberg, Phys. Rev. B **62**, 10 802 (2000).
[46] V. Trepakov, A. Skvortsov, S. Kapphan, L. Jastrabik, and V. Vorlicek, Ferroelectrics **239**, 297 (2000).
[47] G. M. Saley, S. A. Basun, A. A. Kaplyanskii, R. S. Metzler, K. Polgar, and U. Happek, J. Lumin. **87–89**, 1135 (2000).
[48] S. A. Basun, A. A. Kaplyanskii, A. B. Kutsenko, V. Dierolf, T. Tröster, S. E. Kapphan, and K. Polgar, Phys. Solid State **43**, 1043 (2001).